

*This paper is a non-peer reviewed preprint submitted to EarthArXiv.*

**Eocene (50-55 Ma) greenhouse climate recorded in nonmarine rocks of San Diego, CA, USA**

Adrian P. Broz<sup>1,2,5\*</sup>, Devin Pritchard-Peterson<sup>3</sup>, Diogo Noses Spinola<sup>4</sup>, Sarah Schneider<sup>2</sup>, Lucas C.R. Silva<sup>5,6</sup>, and Greg Retallack<sup>2</sup>

<sup>1</sup> Department of Earth, Atmospheric and Planetary Sciences, Purdue University, Lafayette, IN

<sup>2</sup> Department of Earth Sciences, University of Oregon, Eugene, OR

<sup>3</sup> Dudek Environmental Consulting, Encinitas, CA

<sup>4</sup> Department of Chemistry and Biochemistry, University of Alaska, Fairbanks, AK

<sup>5</sup> Environmental Studies Program, University of Oregon, Eugene, OR

<sup>6</sup> Department of Biological Sciences, University of Oregon, Eugene, OR

**\*Correspondence:** [abroz@uoregon.edu](mailto:abroz@uoregon.edu)

*This paper is a non-peer reviewed preprint submitted to EarthArXiv.*

## **Eocene (50-55 Ma) greenhouse climate recorded in nonmarine rocks of San Diego, CA, USA**

Adrian P. Broz<sup>1,2,5\*</sup>, Devin Pritchard-Peterson<sup>3</sup>, Diogo Noses Spinola<sup>4</sup>, Sarah Schneider<sup>2</sup>, Lucas C.R. Silva<sup>5,6</sup>, and Greg Retallack<sup>2</sup>

<sup>1</sup> Department of Earth, Atmospheric and Planetary Sciences, Purdue University, Lafayette, IN

<sup>2</sup> Department of Earth Sciences, University of Oregon, Eugene, OR

<sup>3</sup> Dudek Environmental Consulting, Encinitas, CA

<sup>4</sup> Department of Chemistry and Biochemistry, University of Alaska, Fairbanks, AK

<sup>5</sup> Environmental Studies Program, University of Oregon, Eugene, OR

<sup>6</sup> Department of Biological Sciences, University of Oregon, Eugene, OR

**\*Correspondence:** [abroz@uoregon.edu](mailto:abroz@uoregon.edu)

### **Abstract**

Nonmarine rocks in sea cliffs of southern California store a detailed record of weathering under tropical conditions millions of years ago, where today the climate is much drier and cooler. This work examines early Eocene (50-55 million-year-old) deeply weathered paleosols (ancient, buried soils) exposed in marine terraces of northern San Diego County, California, and uses their geochemistry and mineralogy to reconstruct climate and weathering intensity during early Eocene greenhouse climates. These Eocene warm spikes have been modeled as prequels for ongoing anthropogenic global warming due to atmospheric CO<sub>2</sub> (Anagnostou et al., 2016). Paleocene-Eocene thermal maximum (PETM, ~55 Ma) kaolinitic paleosols developed in volcanoclastic conglomerates are evidence of intense weathering (CIA >98) under warm and wet conditions (mean annual temperature [MAT] of ~17° C ± 4.4° C and mean annual precipitation [MAP] of ~1920 ± 182 mm). Geologically younger Early Eocene climatic optimum (EECO, 50 Ma) high shrink-swell (Vertisol) paleosols developed in coarse sandstones are also intensely weathered (CIA >80) with MAT estimates of ~20° C ± 4.4° C but have lower estimated MAP (~1500 ± 108 mm), suggesting a less tropical climate for the EECO greenhouse spike than for the earlier PETM greenhouse spike.

### **1. Introduction**

Periods of greenhouse conditions, characterized by high atmospheric CO<sub>2</sub> concentrations exceeding ~2000 ppm, punctuated the Earth's climate during the Cenozoic era, from the late Paleocene to the Early Eocene (60 to 52 Myr) (Pearson and Palmer, 2000). During these

periods, global temperatures were often more than ten degrees Celsius higher than those of the pre-industrial period (Anagnostou et al., 2016). These Eocene warm spikes have been modeled as prequels for ongoing anthropogenic global warming due to atmospheric CO<sub>2</sub> (Bowen et al., 2006; Carmichael et al., 2017).

Paleosols (fossil soils) from the Late Paleocene to Eocene periods have been reported worldwide in regions including Antarctica (Spinola et al., 2017), Argentina (Andrews et al., 2017; Sol Raigemborn et al., 2018, 2022), Australia (Zhou et al., 2015), and across the United States (Wilf, 2000; White and Shiebout, 2008, Kelson et al., 2018; These paleosols demonstrate markedly more intense weathering conditions than the present-day environment and are evidence of the warmer climates that prevailed during the early Cenozoic.

New evidence of these warming periods can be seen in a sequence of Eocene paleosols located in today's coastal deserts of southern California, revealing a significantly warmer and wetter paleoclimate. Paleosols in the coastal plains of northwestern Baja California and southwestern California dating back to the pre-Late Eocene age show the effects of intense weathering under a subtropical humid climate (Abbott, 1981). This is consistent with the global greenhouse climates during the Paleocene-Eocene Thermal Maximum (PETM, ~55 Ma) (Kraus et al., 2013; Bowen et al., 2014). An additional global warming event, known as the Early Eocene Climatic Optimum (EECO, 52-50 Ma), also fostered intense weathering in warm, wet climates (Zachos et al., 2008; Song et al., 2018). Despite the recognition of these paleosols for several decades (Abbott, 1981), they are now able to be thoroughly examined using a comprehensive set of climofunctions and other quantitative proxies for soil formation conditions (Sheldon et al., 2002; Sheldon and Tabor, 2009; Nordt and Driese, 2010).

This work uses the morphology, mineralogy and geochemistry of San Diego paleosols to provide a quantitative assessment of climate and weathering intensity on land during and after Eocene greenhouse spikes.

## **2. Geological setting and Cenozoic greenhouse climate**

The study area lies within the peninsular Ranges of southern California and is composed primarily of Jurassic to Cretaceous igneous and metamorphic rocks (Abbott and May, 1991). Orogeny in the mid-Cretaceous led to the formation of a stable, flat-lying coastal-plain stratigraphy that ranges in age from late Cretaceous to early Holocene. This work focuses on two of the coastal plain stratigraphic units of upper Cretaceous and early Eocene age that have preserved evidence of intense subaerial alteration.

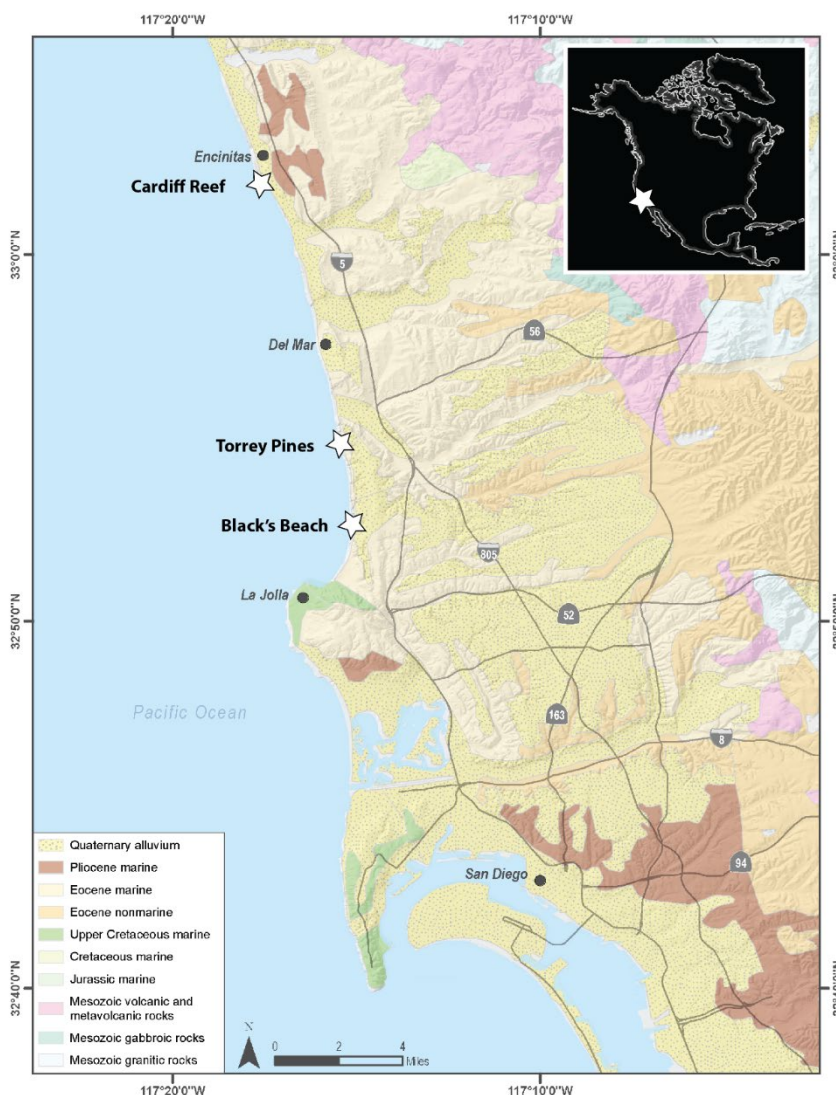


**Figure 1. Field areas in northern San Diego County, California, USA**

Shortly after the late Jurassic to mid-Cretaceous Cordilleran orogeny, San Diego County was transformed into a low-lying coastal plain that accumulated Cretaceous to Cenozoic nonmarine and marine sedimentary deposits (Fredericksen, 1991; Abbott and May 1991). Paleosols of the greater San Diego area developed on Jurassic andesite and andesitic breccia, Rancho Delicias Granodiorite, as well as early Eocene [55 Ma] volcanic and volcanoclastic conglomerates of the Mt. Soledad Formation. The discontinuous sequence of weathered intervals begins with Paleocene (55 Ma) kaolinitic Oxisol paleosols at Rancho Delicias, Tijuana, which are nearly 30 meters in vertical thickness (Abbott, 1981). Approximately 60 km to the north, outcrops of early Eocene (55 Ma) kaolinitic paleosols of the Mt. Soledad conglomerate are exposed in beach cliffs at Black's Beach, La Jolla, below Ardath Shale with mollusks of the *Turritella uvasana* zone (Peterson and Abbott, 1979). These are overlain by Middle Eocene (50 Ma) smectite-rich paleosols of the marginal marine Delmar

formation at San Elijo Beach, Cardiff, CA. Paleosols of the Delmar Formation are overlain by late Eocene (~40 Ma) Aridisol paleosols of the Friars formation that contain abundant pedogenic carbonate nodules and a variety of vertebrate fossils of the Unitan North American Land mammal Age (Abbott, 1981; Walsh et al. 1996). This study focused on paleosols of the early Eocene (55 Ma) Mt. Soledad formation and later early Eocene (50 Ma) Delmar formation. Paleomagnetic evidence locates southern California at latitudes 35-40 ° N during the Paleocene and Early Eocene (Smith and Briden, 1977), at least 400 km north of its current latitude of 32° N.

### **Mount Soledad Formation Conglomerate**

Conglomerates of the basal Mount Soledad formation are overlain by the early Middle Eocene Ardath Shale (Peterson and Abbott, 1979). The Mt. Soledad formation is a framework-supported, amalgamated conglomerate with exotic clast composition (Kennedy and Moore, 1971). The composition of the clasts is dominated by quartz phenocryst-bearing rhyolites that originated from present-day Sonoran desert of Mexico as well as quartzite and silicified tuff (Abbott et al., 1989). The composition ranges from 40% rhyolite, 26% black dacites, 13% Santiago Peak Volcanics, 12% schist, 4% plutonic, and 2% intraformal (Abbott and May, 1991). Paleohydrological reconstruction of the area suggested a 300-km long river with a channel width of 20-80 m and a peak 100-year flood discharge of 30,000 m<sup>3</sup> S<sup>-1</sup> (Abbott, 1981).

### **Delmar Formation Sandstone**

The Eocene (50 Ma) Delmar formation consists of coarse-grained quartzofeldspathic sandstone that was deposited in shallow marine, intertidal and supratidal facies of the Eocene San Diego Embayment (Abbott and May, 1981), and is approximately equivalent in age to the Green River Formation in Wyoming (Smith et al., 2008). Tidally influenced sedimentary features include an assemblage of largely shallow marine oysters, flaser bedding, inclined cross bedding, interlaminated siltstone and mudstone that follow basal and lateral accretionary surfaces of tidal channels, and occasional flood and return-surge deposits (Abbott and May, 1981; Eisenberg and Abbott, 1981). Fossil plants such as giant leather fern (*Acrostichum aureum*) also suggest mangrove habitats (Myers, 1991).

## **3. Materials and Methods**

### **Sample Collection and morphological assessment**

Field descriptions and collection of hand samples was performed at Black's Beach, La Jolla, CA, USA (32.895500, -117.253520) and at San Elijo Beach, Cardiff-by-the-Sea, CA (32.895500, -117.25352) (Figures 2 and 3). Five paleosol profiles were sampled. These included a paleocatena of two profiles (along strike) at La Jolla, and a vertical sequence of three successive profiles in Cardiff. Additional profiles of putative mangrove paleosols in supratidal

facies of the Delmar formation were observed at Torrey Pines, CA and descriptions are included in **Supplementary information (no chemical analyses were performed)**. Hand samples were collected by trenching to approximately 30 cm into the paleosol outcrop for fresh samples. Large, lithified blocks were collected at approximately 20 cm intervals, similar to sampling the horizons of a modern soil profile. The morphology, qualitative grain size, Munsell color and calcareousness of samples were described during collection. Paleosol taxonomic assessment followed the methods and nomenclature of U.S. Soil Taxonomy (Soil Survey Staff, 2014). Pedotypes followed the nomenclature of the local Kumeyaay language spoken by the 12 federally-recognized tribes of the region (Field, 2012).

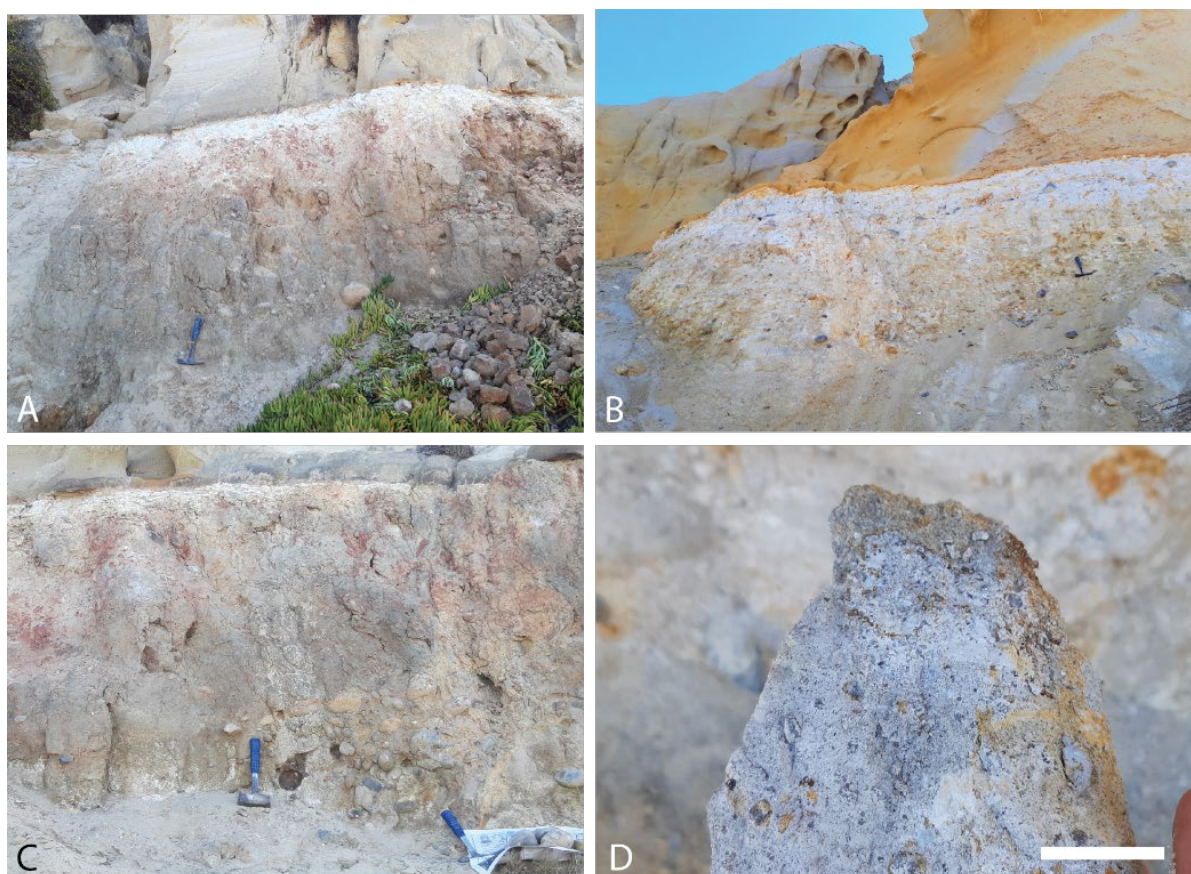


**Figure 2. A paleocatena of two severely weathered early Eocene (55 Ma) kaolinitic paleosols in marine terrace at Black's Beach, La Jolla, California USA (32.895500, -117.253520).** A) White/brown kaolinitic paleosol profile formed in conglomerate of the Eocene (55 Ma) Mt. Soledad formation and buried by overlying Torrey formation sandstone (GPS: ); B) Gray/white kaolinitic profile (along strike) also formed in conglomerates of the Eocene (55 Ma) Mt. Soledad formation and buried by overlying Torrey formation sandstone; C) large >10 cm conglomerate clasts in the C-horizon of the brown/white profile; D) hand sample from the A-horizon of gray/white

profile showing kaolinite (white) and residual coarse quartz clasts. Scale bar in D) is 2 cm

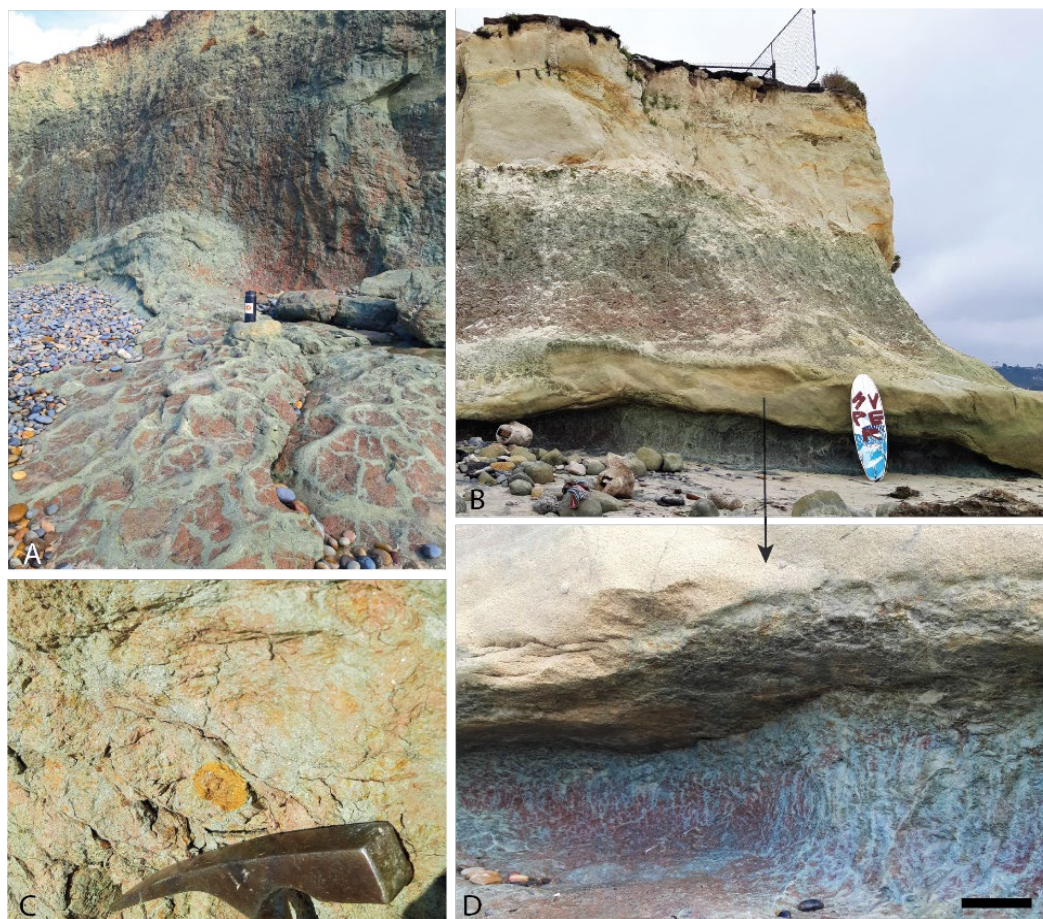


**Figure 3. A sequence of Eocene (50 Ma) red clay Vertisol (shrink-swell) paleosols at San Elijo Beach, Cardiff-by-the-sea, California, USA (32.895500, -117.25352).** A) Three successive Vertisol paleosols exposed in marine terraces with soil structures exposed in the shore platform including coarse sand-filled mudcracks; C) common Fe oxide concretions up to 5 cm in diameter in the B-horizons of the lowermost two profiles; D) Drab green/gray coarse sand-filled mudcracks and brick-red matrix of the basal paleosol profile with extensive mottling extending to sea in the shore platform. Scale bar in C) is 10 cm

### **Bulk geochemistry**

Major element chemistry of paleosols was determined by X-ray fluorescence and Pratt titration for FeO at ALS Laboratories, Vancouver, British Columbia (Table S1). These data were used to calculate molar weathering ratios, indices of alteration, and geochemical mass

balance (tau, strain) of each paleosol profile. Bulk density was measured on lithified clasts using the paraffin-clod method of Blake and Hartge (1986). These values are provided in Tables S1 and S2.

### **Geochemical Proxies**

The degree of weathering of paleosols can be estimated using molecular ratios as indicators of the soil-forming processes (Retallack, 2019) including salinization ( $\text{Na}_2\text{O}/\text{K}_2\text{O}$ ), calcification ( $\text{CaO} + \text{MgO}/\text{Al}_2\text{O}_3$ ), clayeyness ( $\text{Al}_2\text{O}_3/\text{SiO}_2$ ), base loss ( $\text{Al}_2\text{O}_3/\text{CaO} + \text{MgO} + \text{Na}_2\text{O} + \text{K}_2\text{O}$ ) and gleization ( $\text{FeO}/\text{Fe}_2\text{O}_3$ ). Salinization is a measure of the salt accumulation in paleosols whereas calcification estimates the accumulation of pedogenic carbonates at depth. Clayeyness and base loss evaluate the extent of hydrolytic weathering and leaching of cations as a function of depth in the profile. Gleization constrains the redox state of the soil before burial, with values  $> 1$  suggesting waterlogged and reducing conditions and values  $< 1$  suggesting well-drained, oxidizing conditions before burial (Retallack, 2019; Broz, 2020). Oxide weight percentages were also used to estimate mean annual precipitation using the CIA-K (chemical index of alteration minus  $\text{K}_2\text{O}$ ) paleoprecipitation proxy (Sheldon et al., 2002), defined as  $221.12e^{0.0197(\text{CIA-K})}$  with  $R^2$  0.72 and standard error (s.e.) of 182 mm, and the CALMAG weathering index, designed for use with Vertisol paleosols (Norse and Driese, 2010), defined as  $\text{Al}_2\text{O}_3/(\text{Al}_2\text{O}_3 + \text{CaO} + \text{MgO}) \times 100$ . The CALMAG paleoprecipitation proxy ( $y=22.69x - 435.8$ ,  $R^2 = 0.90$ ; s.e.  $\pm 108$  mm, where  $x =$  CALMAG weathering index) was compared with CIA-K paleoprecipitation estimates (Sheldon et al., 2002). Calculated values are provided in Table S3.

### **Total Inorganic / Organic carbon and pH**

The pH and total organic carbon (TOC) of samples was assessed to constrain the organic content and diagenetic history of paleosols. Since waterlogged soils can be sites of enhanced organic preservation, especially those with  $\text{FeO}/\text{Fe}_2\text{O}_3 < 1$  (Broz et al, 2022), we used elemental analysis to quantify the paleosol organic carbon pool. However, paleosols often contain both ancient and modern carbon as inferred from radiocarbon dating, and distinguishing between the two can be challenging (Broz et al., 2022). Furthermore, reconstructing soil pH from paleosols is difficult because diagenesis (e.g., groundwater alteration) can obscure or overprint original soil pH (Lukens et al., 2018). Paleosol samples were then manually encapsulated in  $5 \times 8$  mm tin capsules (sample size approximately (25–70 mg) prior to elemental analysis. Total organic carbon was determined by elemental analysis on a Costech ECS 4010 instrument at the University of Oregon's Soil-Plant-Atmosphere Laboratory, with expected standard deviation  $< 0.3\%$ . Paleosol pH was determined by electrode in a 1:2 mixture of ground paleosol sample to deionized water. No pre-acidification of paleosols were performed here (e.g., Harris et al., 2001), so it is possible that paleosols with



pH >6.5 have some amount of inorganic carbon (e.g., carbonate). All samples were analyzed in duplicate. TOC and pH values are provided in Table S4.

### **Visible/near infrared spectroscopy**

Visible-near infrared (VNIR) spectroscopy was used to determine the alteration mineralogy of select samples. Lithified hand samples of paleosols (approximately 200 g) were selected for analysis. An ASD FieldSpec Pro3 reflectance spectrometer in the Planetary Surfaces Laboratory at Purdue University was used to examine the reflectance spectra of samples from 0.35-2.50  $\mu\text{m}$ . Samples were not ground or sieved before analysis. Spectra from laboratory standards of kaolinite, hematite, goethite, montmorillonite and illite from the Western Washington University Vis-NIR Spectroscopy Database were compared with spectra from hand samples to constrain the mineralogy of unknown samples. Raw spectra are provided in Table S6.

### **Micromorphology**

Petrographic thin sections of paleosol samples were used to classify paleosol micromorphology, estimate grain size distribution and constrain mineral composition (Murphy, 1983). Thin sections of oriented paleosol samples were point counted using a Swift automated stage and Hacker counting box fitted to a Leitz Orthoplan Pol research microscope. Determination of average grain size and qualitative mineralogy with error of 2% for common components (Murphy (1983). A total of 1000 points on each thin section were counted (500 points for relative proportion of minerals and 500 points for determination of sand, silt and clay size fractions) (**Table S7**). Thin section descriptions followed methodology outlined by Stoops (2003). Focus was given to pedogenic features indicative of soil forming processes (e.g., clay coatings and nodules) as well as to b-fabrics.

## **4. Results and Discussion**

### **4.1 Morphology and micromorphology**

#### ***Mshap* (White) profile**

The kaolinite-rich profile analyzed in this study, hereby referred to as *Mshap* ("White" in the Kumeyaay language; Field, 2012), exhibits characteristics consistent with a poorly-drained Ultisol paleosol, known as an Aquult soil in US Soil Taxonomy System (Soil Survey Staff, 2014). This profile has a kaolinitic E-horizon that gradually transitions into a well-developed, mottled B horizon distinguished by large (10 cm length) drab-haloed root traces. The bleached E horizon subtly grades into the mottled red hues of the B horizon (Figure 4), a transition suggesting intermittent saturation potentially caused by seasonal flooding. The deepest horizon (C) hosts a parent material of well-rounded chert and quartzite clasts, imbricated to the west, with diameters reaching up to 15 cm. The A-horizon of the original profile was likely removed by erosion during the deposition of the overlying sandstone. It appears that

weathered conglomerate clasts extend deeper into the C-horizon of the profile (possibly 3-4 meters), but views of such material were obscured by colluvium at the time profiles were observed (e.g., unweathered R-horizon of conglomerate at bottom of profile was covered by overburden and not visible), so it is possible that profiles are indeed ~3-4 meters or more in vertical thickness as noted by Abbott (1981).

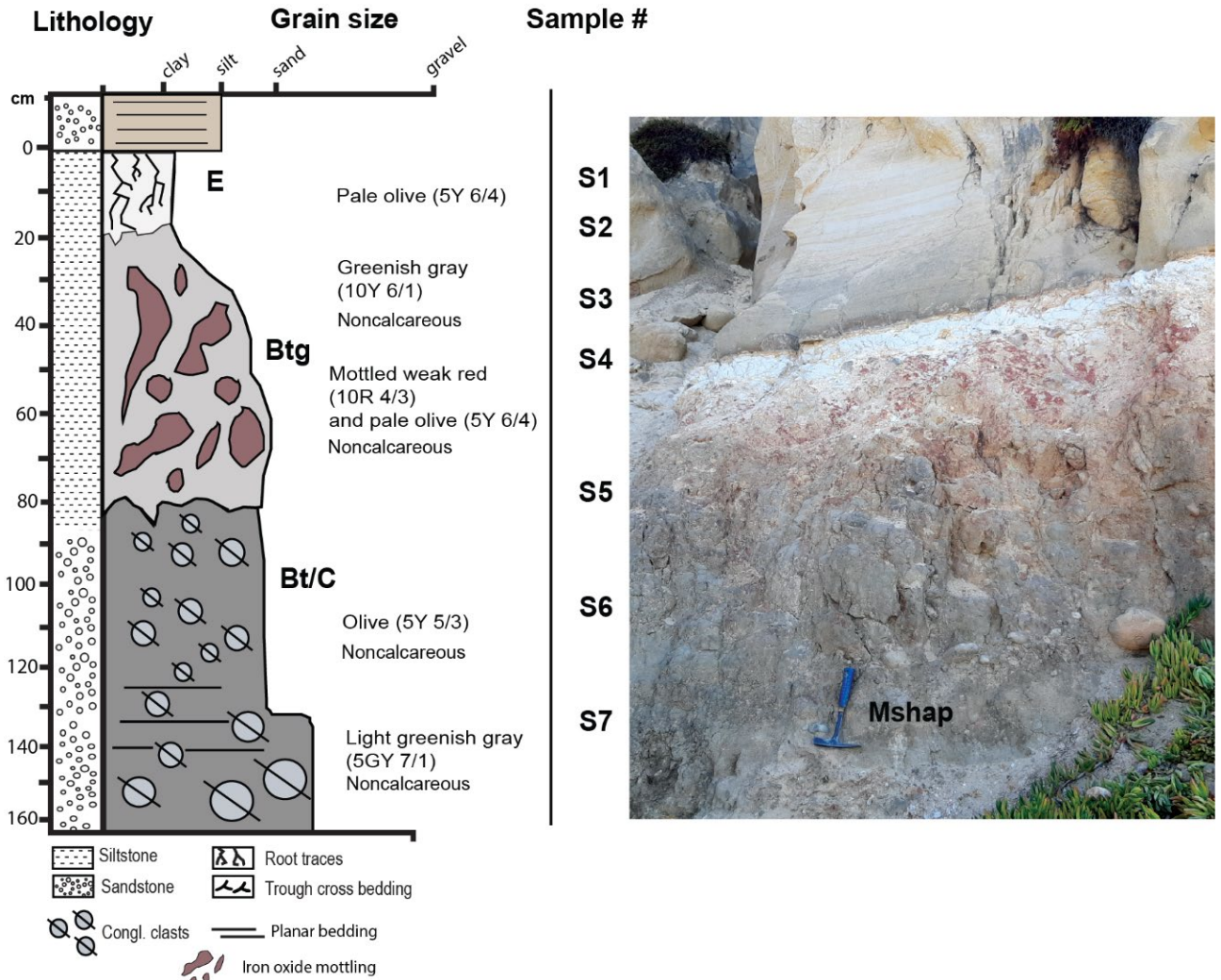


**Figure 4. Well-drained *Mshap* Inceptisol paleosol (Tropept) at Black’s Beach, La Jolla, CA, with a kaolinitic A-horizon and a mottled Bw horizon with large drab-haloed root traces. The C horizon has rounded chert and quartzite clasts up to 15 cm in diameter that are imbricated to the west. All clasts are well rounded.**

Micromorphological observations also support the hypothesis of an Aquult-like paleosol (Table S8). The surface horizon visible in the outcrop has been identified as an E horizon, characterized by clay and Fe depletion. A few clay coating remnants were observed in several planar voids (Figure 5), while the subsurface horizons exhibited an abundance of clay coatings and redoximorphic features (Figure 5).

The subsurface horizons have been classified as a sequence of poorly-drained argillic (Btg) horizons, primarily due to the frequent presence of clay coatings, Fe nodules, and depletion/impregnation features (Figure 5). The clay coatings were limpid, displaying low interference colors. These coatings were frequently found associated with planar voids and showed clear extinction lines, although signs of occasional disturbance such as fragmentation and poor orientation were evident. We hypothesize that pedoturbation—via the incorporation of clay coatings into a clayey groundmass—and post-burial deformation may have been contributing factors to the disturbance of clay coatings. The presence of striated b-fabrics (e.g., grano, cross, and circular) in the B horizons supports the suggestion of substantial pedoturbation processes (Figure 5) (Kühn et al., 2018).

There was no evidence of lithological discontinuity, suggesting a continuous profile. The uniformity of the parent material across all samples is indicated by the similar c/f distribution, mineral composition, roundness, and sorting (Table S8). Quartz, which dominates the coarse fraction, displays a predominantly wavy extinction, hinting at a metamorphic origin. The intense weathering present was confirmed by the detection of runiquartz (Table S8)

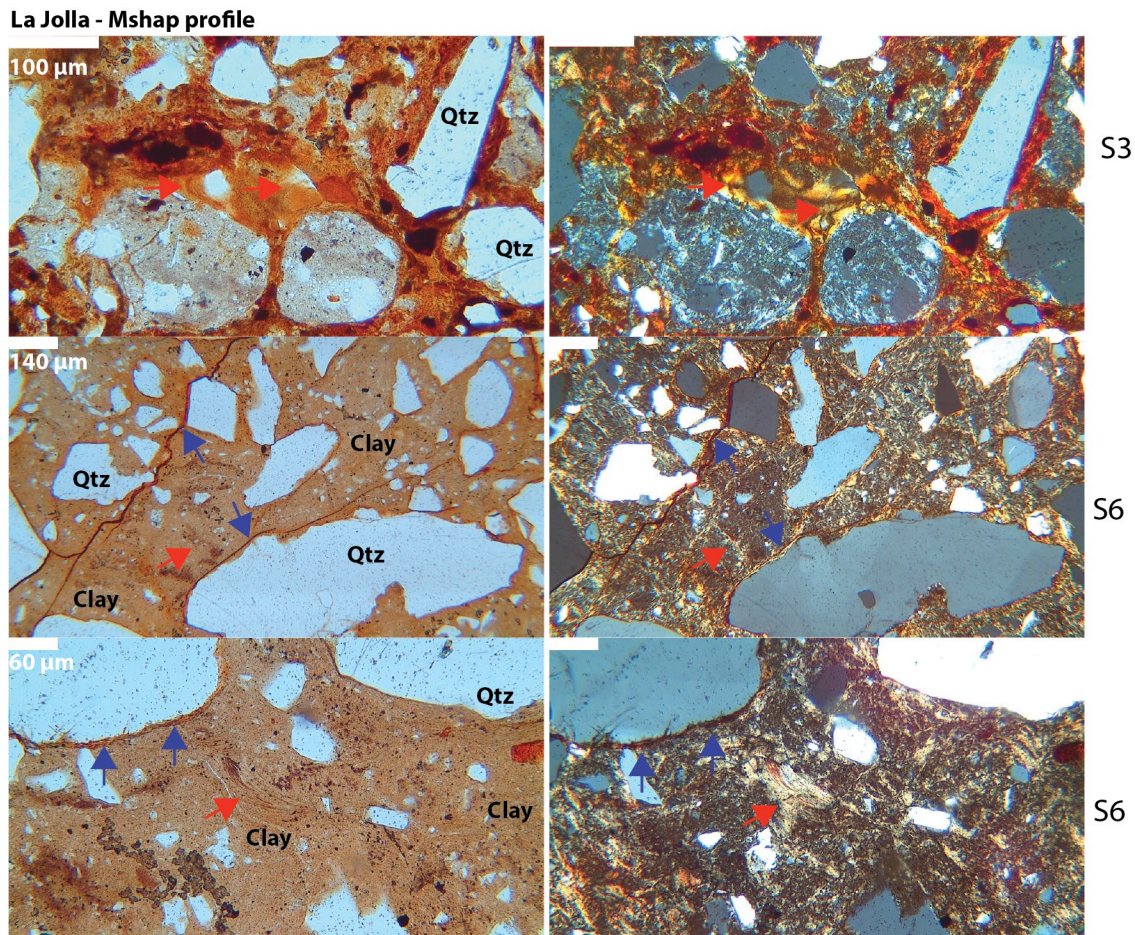


**Figure 5. Micromorphological features of the early Eocene (55 Ma) La Jolla (*Mshap*) profile seen in plane polarized light (PPL, left column) and cross polarized light (XPL, right column). Top row is E horizon showing limpid and oriented clay coatings (red**

arrows) and Fe nodules (dark spots in PPL/XPL); middle row is Btg horizon showing circular striated b-fabric (red arrow) and granostriated b-fabrics with limp and oriented clay coatings (blue arrows); bottom row is Btg horizon showing clay coatings (red arrow) and Fe hypocoatings (blue arrows). Sample nomenclature in right column can be traced across all analyses performed on samples (see Tables S1-S9)

### ***Hwatt (red) profile***

This profile at La Jolla resembled a poorly-drained Inceptisol paleosol (Aquept). Because of the common and large red mottles, it is herein *referred to as Hwatt* ("Red" in the Kumeyaay language). The bleached-white kaolinitic A-horizon contained root traces up to 2 cm in diameter and reaching 18 cm in depth. This profile also has a kaolinitic A-horizon overlying a mottled Bw horizon with rounded quartzite clasts up to 15 cm in diameter and a mixture of sand and clay. The gray to white subsurface (B) horizon was consistent with poorly drained conditions indicated by the bleached surface grading into a mottled red subsurface indicative of seasonal waterlogging (Retallack et al., 2001). The C horizon contains well-rounded chert and quartzite clasts also imbricated to the west and up to 20 cm in diameter. The pair of paleosols described at Black's Beach represent a paleocatena, two soils varying laterally (along strike) from the same ancient land surface, representing differences in paleotopography (e.g., hillslope vs. toeslope) (Retallack, 2019).

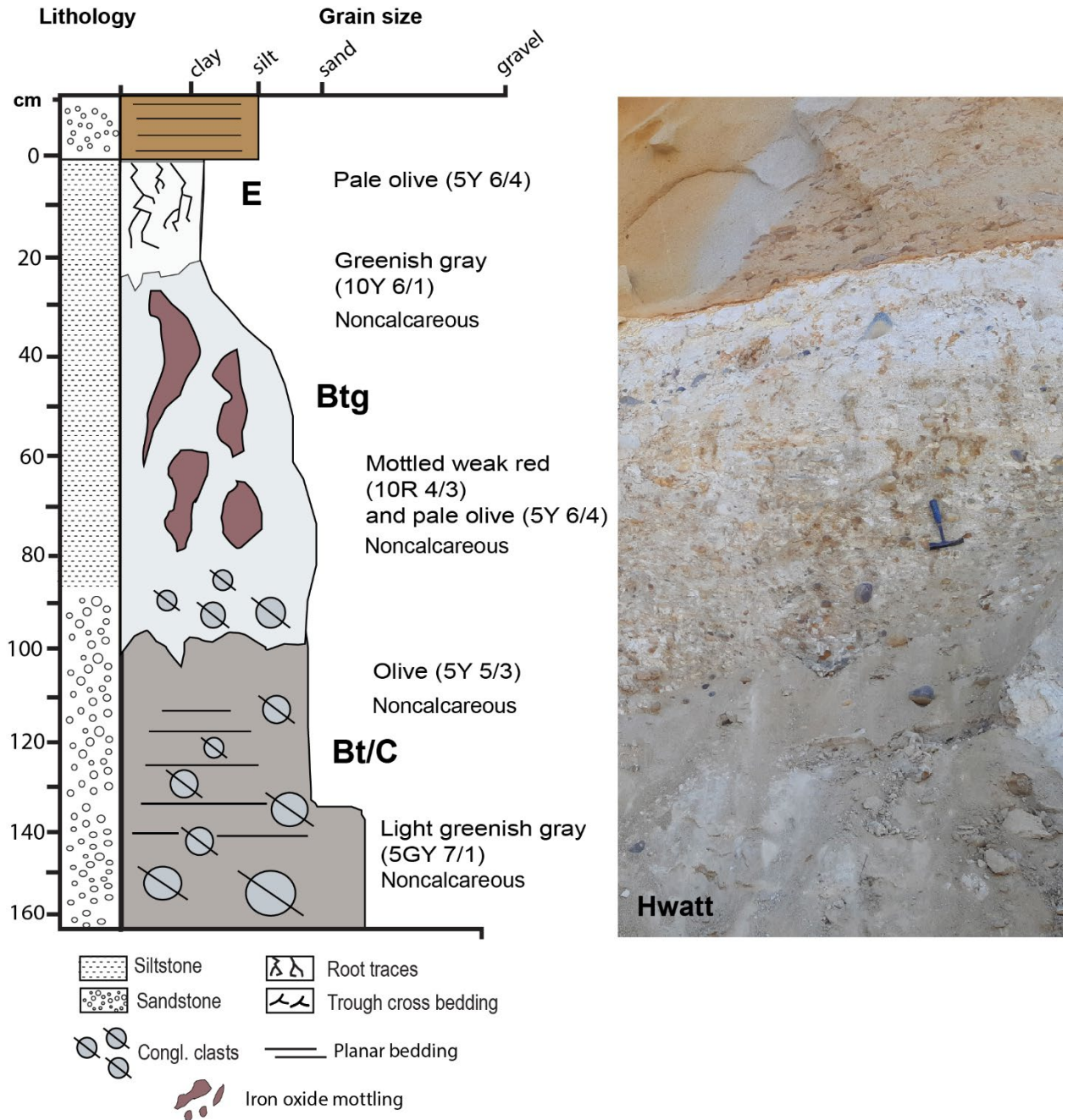


**Figure 6. Poorly drained *Hwatt* paleosol (Aquult) at Black's Beach, La Jolla, CA** with root traces up to 2 cm in diameter and reaching to 18 cm in depth. This profile also has a kaolinitic A-horizon overlying a mottled Bw horizon with rounded quartzite clasts up to 15 cm in diameter.

### ***Psiiw* (Green) and *Hamulh* (Surf) profiles**

This sequence of three clay-rich paleosols at Cardiff resembled a modern Vertisol (smectitic high shrink-swell soils) (Soil Survey Staff, 2014), which formed on a parent material of

quartzofeldspathic sand. The uppermost two profiles, herein referred to as *Psiiw* or “green” in Kumeyaay language (Field, 2012) overlie the basal *Hamulh* (“Surf”) pedotype that composes the shore platform and extends seaward. The weak red (10R 5/4) surface horizons contain common and massive, sand-filled polygonal desiccation features, common slickenslides oriented at random angles, and abundant drab halo root traces to 4 cm in diameter and up to 25 cm in depth. These graded into a weak red (10R 5/4) subsurface clay horizons (Bss or Bssg horizons) also with abundant slickenslides, occasional clasts of coarse quartz sand, and occasional Fe concretions up to 3 cm in diameter (Figure 7). The ledge-forming BC-horizon of the middle profile was a light greenish gray (10Y 7/1) noncalcareous coarse-grained quartzofeldspathic sandstone. This overlaid the basal profile, which was brick red (10 R 5/4) and also pierced with mottled green (10Y 8/1) sand-filled cracks and root traces to 5 cm in diameter with abundant slickensides. Large (75 cm depth and up to 10 cm in diameter), polygonal, sand-filled mudcracks are common in other Vertisol paleosols (Driese and Foreman, 1992; Driese and Ober, 2005).

The basal *Hamulh* paleosol profile in the shore platform extends seaward (Figure 3) and creates “Cardiff Reef”, a world-famous surfing area known for long, tapering and consistent wave formation, due in part to incision of the shore platform by the San Elijo river (**Figure S1**) that has created a deep offshore channel located approximately 50 m south of the Cardiff study area (Ludka et al., 2019).

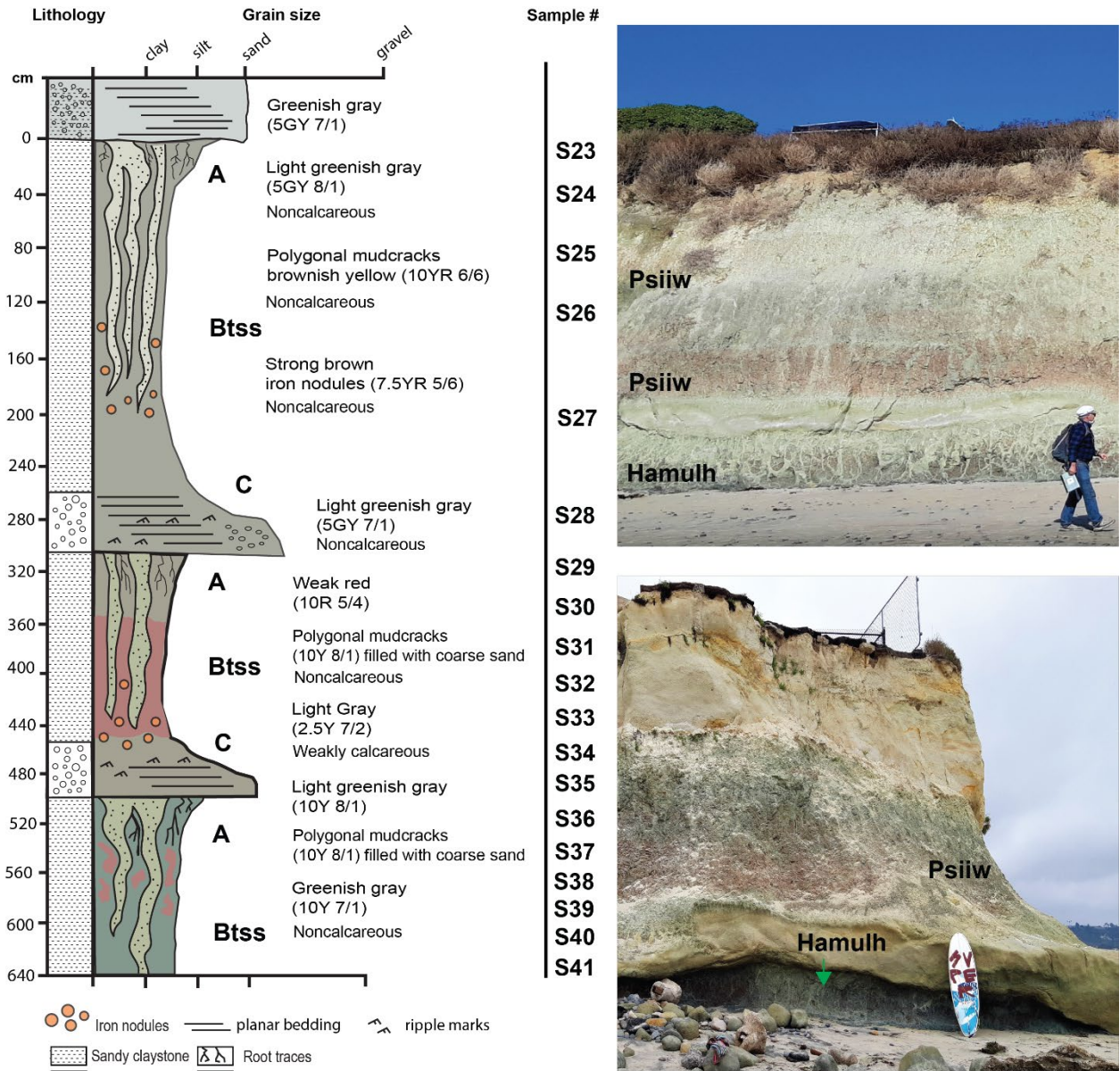


**Figure 7. Sequence of red clay Vertisol (shrink-swell) paleosols in beach cliffs and shore platform at San Elijo Beach, Cardiff, CA.** Deep (<75 cm) coarse-sand-filled polygonal mudcracks are green/gray in color (10Y 8/1) and are present in weak red (10R 5/4) soil matrix with abundant slickensides and Fe-bearing concretions.

Micromorphological observations validated the formation of a paleo-Vertisol (Figure 8). Diagnostic vertic soil properties, including a large and well-developed blocky structure along with strongly striated b-fabrics, were consistently observed throughout the Bss horizons (Figure 8) (Kovda and Mermut, 2018).

The A horizons were characterized by a smaller blocky structure with a secondary granular structure, accompanied by a well-developed pore network resembling fine roots,

which likely belonged to a grassland-type vegetation. The infilling of finer textured particles in larger pores suggested proximity to the surface (Figure 8, top row).

We identified lithological discontinuities and buried horizons, as denoted by the numerical prefix in the horizon designations and the "b" suffix, respectively. The lithological discontinuities were readily discernible due to abrupt alterations in the size, sorting, and composition of the coarse fraction. The buried horizons were identified by the sudden reappearance of A horizon properties, such as an extensively developed pore system resembling roots and material infilling.

Overall, this paleosol sequence demonstrated relatively good drainage, and only a few horizons showed redoximorphic features like Fe coatings, nodules, and an Fe-depleted groundmass (Fig. X). Unlike the La Jolla profiles, the Cardiff profiles demonstrated a more diverse mineral composition, predominantly featuring quartz with a frequent occurrence of biotite and plagioclase. Notably, no instances of runiquartz formation were detected.

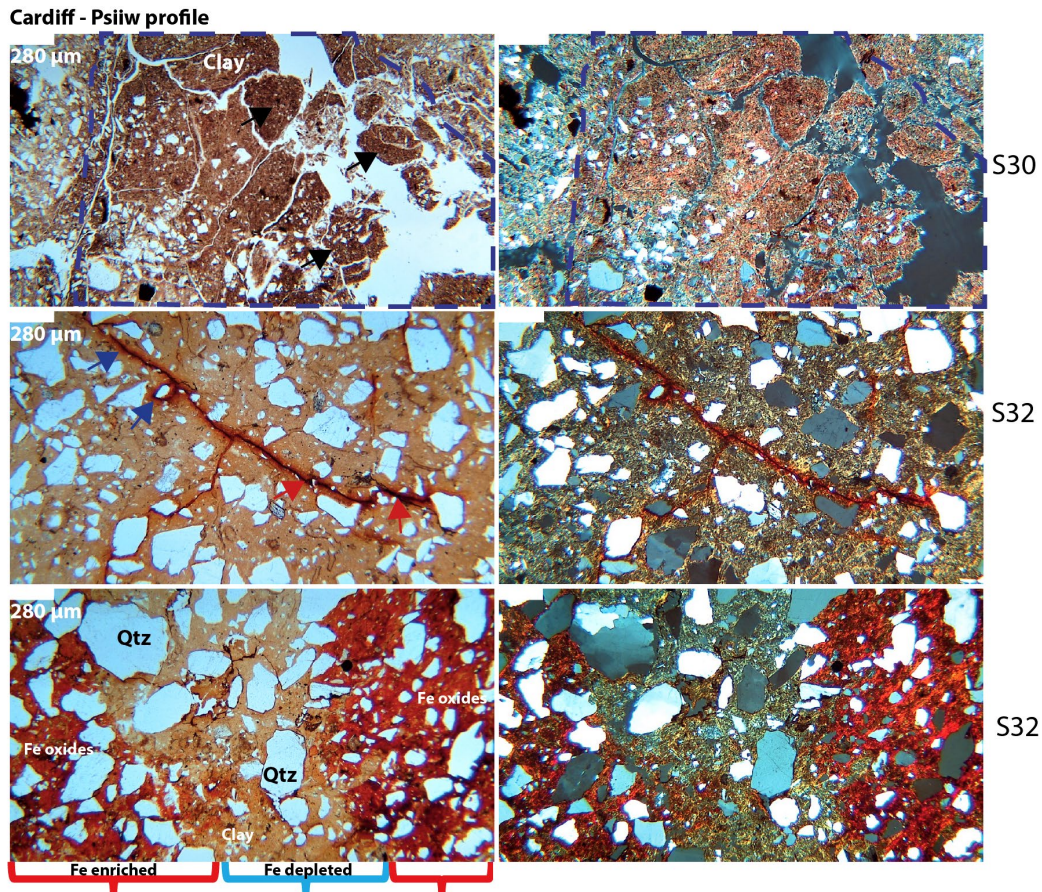


**Figure 8. Micromorphological features of the Eocene (50 Ma) Cardiff (Psiw) profile seen in plane polarized light (PPL, left column) and cross polarized light (XPL, right column).** Top row shows A-horizon with subangular blocky ped structure (black arrows) and clay mineral accumulation; note well developed-pore network with finer material indicated by dashed blue line; middle row shows Btss horizon with well-developed b-fabric (yellow in PPL) and Fe-oxide lined pore network; red arrows indicate inner Fe matrix and blue



arrows indicate outer diffuse Fe matrix boundary; bottom row shows Btss horizon with residual quartz and Fe enriched areas (red brackets) alternating with Fe depleted areas (blue bracket). Sample nomenclature in right column can be traced across all analyses performed on samples (Tables S1-S9)

### **Visible/near infrared spectroscopy**

Analysis of the La Jolla paleosol (Mshap) showed strong absorptions with band centers near 0.5, 0.8, 1.41, 1.9, 2.16, 2.2, and 2.39  $\mu\text{m}$  (Figure 9). We interpret these absorptions as kaolin-group minerals (kaolinite, halloysite, dickite) with contributions from Fe oxides and a  $\text{Fe}^{3+}$ -bearing phyllosilicate. The absorptions at 1.41  $\mu\text{m}$  are indicative of the first kaolinite overtone whereas the 1.9  $\mu\text{m}$  band is from a combination tone of Al-OH bending and H-O-H stretching in  $\text{H}_2\text{O}$  (Goudge et al., 2015) or from the presence of another hydrated phase. A shoulder exists at 2.16 as a doublet with the 2.20  $\mu\text{m}$  band, which is caused by a combination tone of the OH stretch (Bishop et al., 2008) and is diagnostic of kaolinite (**e.g., Ye and Michalski, 2022**). A band near 2.39  $\mu\text{m}$  could also be consistent with OH stretching and bending combinations in a  $\text{Fe}^{3+}$  phyllosilicate, possibly due to the isomorphic substitution of Al or Fe for Si in the tetrahedral layers, or from cation bonding between tetrahedral and octahedral layers (Bishop et al., 2008).

The presence of finely crystalline Fe oxides in the lower Mshap profile was inferred from absorption features centered near 0.5  $\mu\text{m}$  and a broad feature near 0.85  $\mu\text{m}$  (Haber et al., 2022). The C horizon had the most pronounced Fe oxide features with the largest band depth at 0.85  $\mu\text{m}$  noted across all samples. Fe oxides features were mainly observed in the subsurface horizons and were absent in the surface (E horizon) samples. This suggests that the surface horizon may have been poorly drained and chemically reducing whereas the subsurface may have been well-drained and more oxidized.

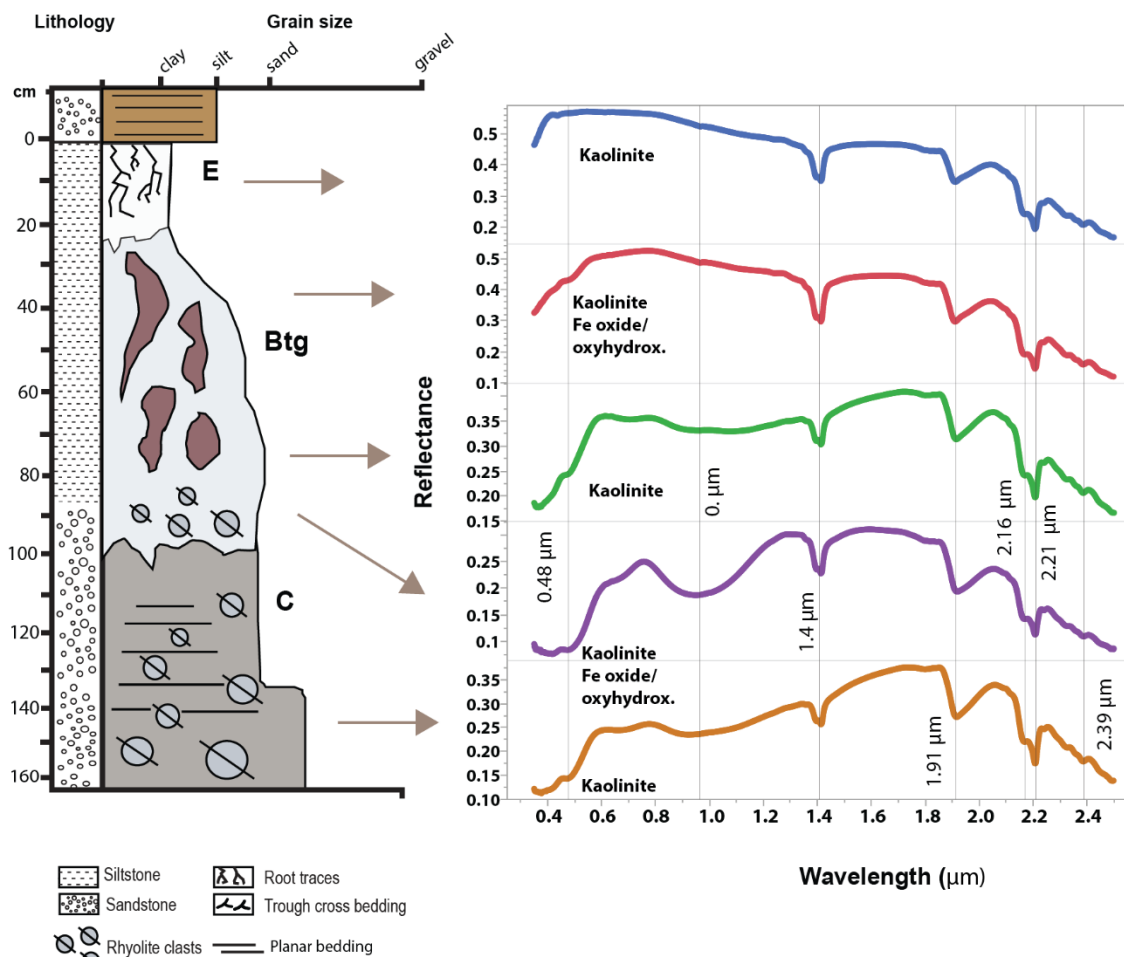


**Figure 9. Visible-near infrared spectroscopy of the La Jolla Ultisol paleosol.**

Absorption features highlighted at 0.48, 0.97, 1.4, 1.95, as well as the doublet feature at 2.16 and 2.2  $\mu\text{m}$ , are consistent with kaolinite and Fe oxides and/or oxyhydroxides

The Cardiff paleosols had absorptions with band centers at 1.4, 1.91, 2.21 and  $\sim 2.35$   $\mu\text{m}$ . The absorption features at 1.91 and 2.21  $\mu\text{m}$  were consistent with a strongly crystalline Al smectite (e.g., Al montmorillonite). The absorptions at 1.4  $\mu\text{m}$  and 1.9  $\mu\text{m}$  were similar to kaolinite, but the kaolinite-diagnostic doublet feature at 2.16 and 2.2  $\mu\text{m}$  was absent in all but one of the Cardiff samples. Instead, an absorption feature near  $\sim 2.35$   $\mu\text{m}$  was consistent with  $\text{Fe}^{2+}$ -rich phyllosilicates such as zinnwaldite and/or chamosite, or a mixed layer illite-smectite (Bishop et al., 2008).

Despite the extensive green-red mottling in the Cardiff paleosols, Fe oxide signatures were largely absent in the visible wavelengths. Only one sample, the A-horizon of the lowermost profile, had absorption features centered near 0.5 and 0.8  $\mu\text{m}$ , characteristic of Fe oxides such as hematite. Interestingly, the lowermost profile was the reddest of the three profiles and suggested it may have been less affected by early diagenetic burial gleization (Retallack, 1991). This process may have converted a significant portion of the Fe oxides and

oxyhydroxides from the ferric state to a drab-colored ferrous state, and since ferrous iron is much more soluble, may have resulted in depletion of total iron in the profiles (Retallack, 1991). This may be why we did not see strong Fe oxide signatures in most samples despite the inferred presence of ferric iron characteristic of deeply weathered soils (Brown et al., 2006).

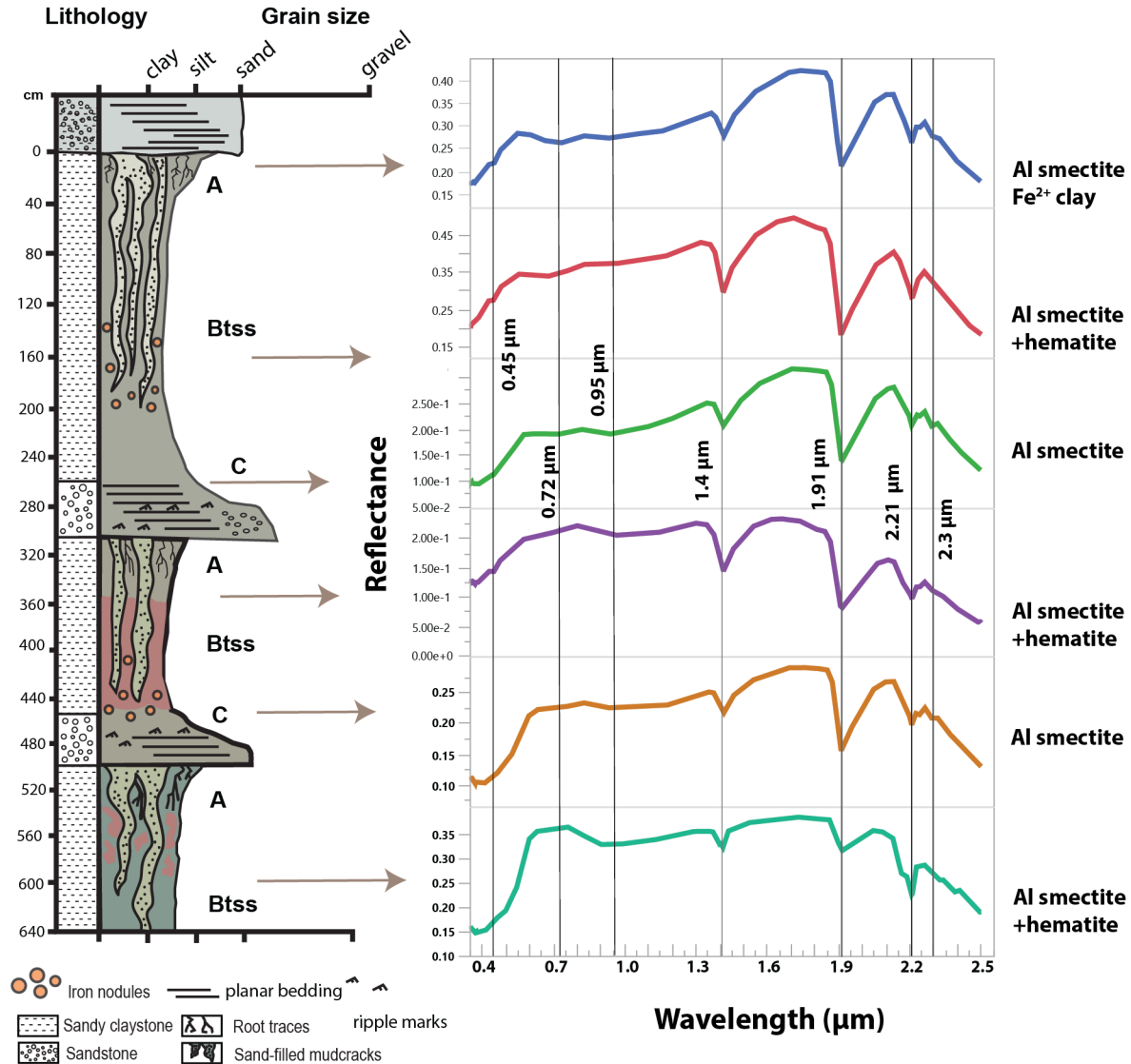


**Figure 10. Visible-near infrared spectroscopy of three Vertisol paleosol profiles from Cardiff-by-the-sea, CA.** Absorption features highlighted at 0.45, 0.74, 1.4, 1.91, 2.21 and 2.3 μm are consistent with Al smectite and hematite

Paleosols at both localities showed chemical weathering trends consistent with extensive leaching and subaerial alteration (Figure 11). The *Hwatt* Ultisol-like paleosol (La Jolla) showed only slight salinization ( $\text{Na}_2\text{O}/\text{K}_2\text{O}$ ) and calcification ( $\text{CaO}+\text{MgO}/\text{Al}_2\text{O}_3$ ) with values less than 0.15 (Figure 11A). On the other hand, we observed moderate clayeyness ( $\text{Al}_2\text{O}_3/\text{SiO}_2$ ) in the uppermost horizon with values up to 0.4 that decreased to 0.2 in the subsurface (Bt and C)

horizons. Base loss followed a similar trend where the highest values (~40) were noted in the near-surface horizons and decreased to values less than 20 in the C horizon. Gleization, indicative of waterlogging before burial, was greatest in the surface (E) horizon and decreased with depth. Low salinization and calcification values (~0.1) were noted and are common in Ultisols of wet climates where precipitation exceeds evapotranspiration (Retallack, 2019). Clayeyness and base loss were highest in the near-surface horizons of the paleosol, indicative of subaerial alteration and leaching, but overall values were less than would be expected for a more deeply weathered Oxisol. Gleization values of ~0.5 in the A-horizon also suggest waterlogging conditions before burial and are consistent with seasonal saturation by surface water. A decrease of FeO/Fe<sub>2</sub>O<sub>3</sub> in the subsurface horizons suggests surface water rather than groundwater was responsible for the seasonal waterlogging conditions.

### **Chemical Weathering Trends**

The Cardiff Vertisol paleosols (*Psiiw and Ha Mulh*) had salinization and calcification values up to ~4 and 0.2, respectively, with the highest values in the A horizons of both profiles (Figure 11B). Moderate salinization suggests that precipitation was not adequate to remove most Na<sub>2</sub>O, especially when compared to the low salinization values of the La Jolla (*Hwatt*) profile. Low calcification values (up to 0.2) were similar to the Hwatt profile, suggesting an absence of pedogenic carbonate. Vertisols of wet climates such as those examined here (MAP > ~1000 mm) do not typically contain pedogenic carbonate whereas Vertisols of dry climates (MAP < 1000 mm) can accumulate pedogenic carbonate in subsurface (i.e., B<sub>ssk</sub>) horizons (Driese et al., 2000), leading to increased calcification values (Retallack, 2019). On the other hand, base loss in the Cardiff Vertisols was an order of magnitude lower than the Hwatt paleosol (base loss values of 1-4 versus 40). These base loss values are consistent with other observations of Cambrian Vertisol paleosols from South Australia (Retallack, 2009) and suggest lower weathering intensity compared to the *Hwatt* profile. Lastly, gleization was highest in the paleosurface horizons of both profiles, suggesting either seasonal saturation during pedogenesis or burial-induced diagenesis such as burial gleization (PiPujol and Buurman, 1994). Burial gleization is envisaged as the reduction of Fe by anaerobic microbes shortly after burial (Broz et al., 2022). In both cases, accumulation of FeO is limited to the near-surface horizons (e.g., the paleosurface).

### **Chemical Index of Alteration**

The geochemistry of the La Jolla paleosol showed extensive depletion of mobile cations (Ca, Mg, K, Na) and a chemical index of alteration minus potassium (CIA-K) of >98 in the near-surface horizon (Figure 11A). The profile was nearly devoid of all mobile cations and was significantly enriched in Si and Al. The paleosurface horizons (A and B<sub>t</sub>) had the highest CIA-K observed in the study with average values of ~99 that decreased to ~93 in the subsurface

(Bt/C) horizon. These high CIA values are indicative of nearly complete kaolinitization, typical of highly weathered soils and paleosols (Nesbitt and Young, 1982; Babechuk et al., 2014).

The Cardiff paleosol sequence (50 Ma) was less intensely weathered relative to the Eocene La Jolla paleosol (55 Ma), though with significant depletion of Ca, Mg, K, and Na, and CIA-K values ranging from ~77-88 (Figure 11B). The CIA was greatest in the lower A and upper Bss horizons of both profiles. Though not as intensely weathered relative to the La Jolla paleosol, the accumulation of Fe oxides and massive vertic features including sand-filled cracks also indicate extensive leaching under a warm, humid and seasonally dry climate. The less intense weathering of Cardiff paleosols were supported by micromorphological observations where biotite and plagioclase were detected, while only quartz was detected in the La Jolla paleosols.

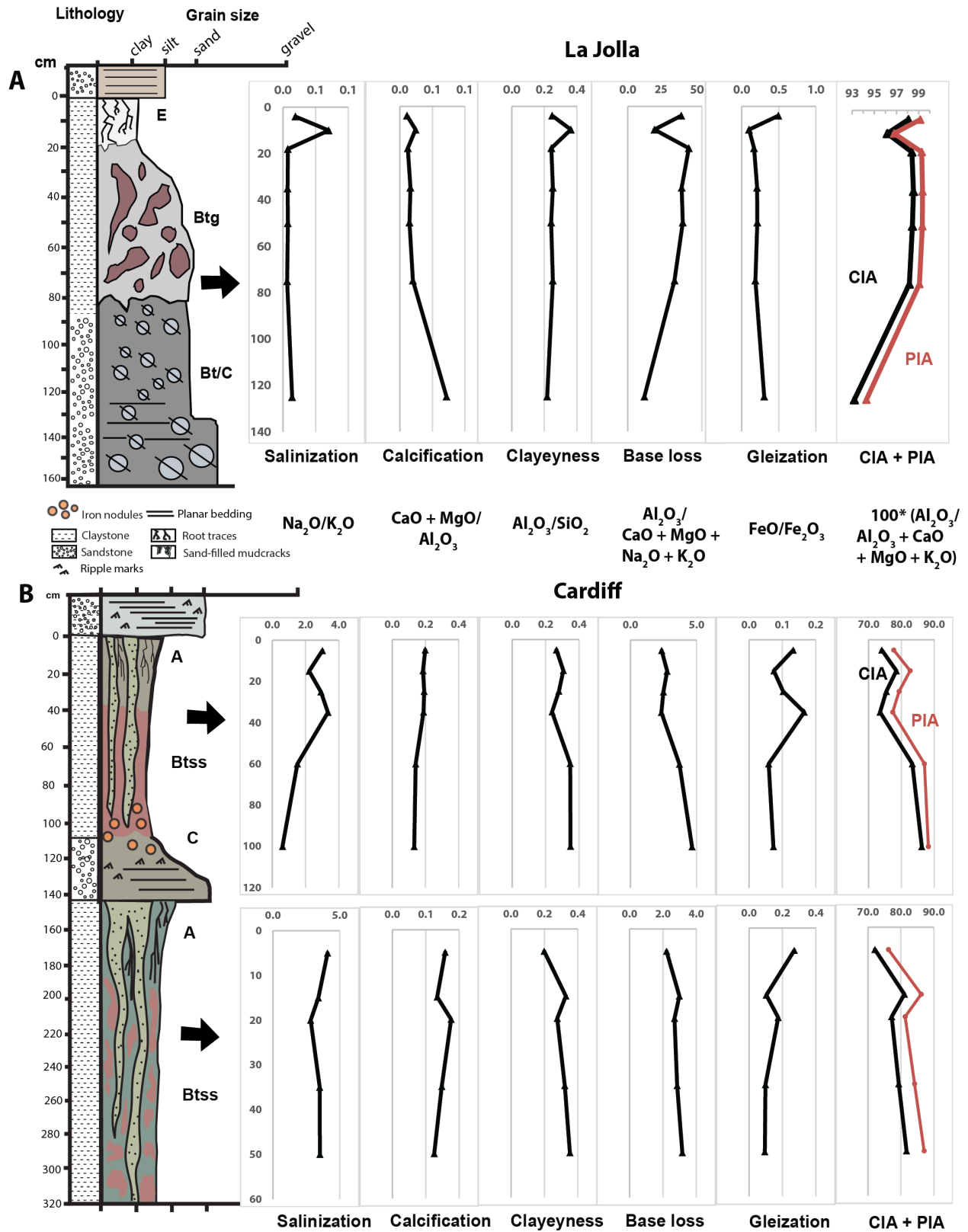


**Figure 11. Geochemical trends of paleosols from La Jolla and Cardiff-by-the-Sea, CA. A)** Geochemical trends with depth in a kaolinitic Ultisol from Black's Beach, La Jolla, CA; and **B)**

Vertisol (high shrink-swell) paleosols from San Elijo Beach, Cardiff by-the-sea, CA. CIA, Chemical index of alteration ( $100 \times [\text{Al}_2\text{O}_3 / (\text{Al}_2\text{O}_3 + \text{MgO} + \text{CaO} + \text{K}_2\text{O})]$ ); PIA, Plagioclase index of alteration ( $100 \times [\text{Al}_2\text{O}_3 - \text{K}_2\text{O} / (\text{Al}_2\text{O}_3 + \text{MgO} + \text{CaO} - \text{K}_2\text{O})]$ )

La Jolla Ultisol paleosols had total organic carbon (TOC) ranging from 0.026 - 0.079 ( $\pm 0.003$ ) wt. % and pH ranging from 3.523 - 6.283 ( $\pm 0.018$ ), indicating highly acidic tropical weathering conditions (**Table S2**). Like modern soil profiles, the organic carbon content was enriched in the surface horizons of paleosols (E horizon) and subsequently depleted in the lower horizon (C horizon). It should be noted that paleosol pH is often compromised by late-stage groundwater alteration, which can reset the original pH (Lukens et al., 2018), so caution is needed for primary interpretation of paleo-pH reconstruction. However, modern Oxisols and Ultisols are characterized by low pH as a result of intense weathering and the generation of organic acids (Lawrence et al., 2013; Driese et al., 2018), so perhaps the pH values we measured represent minimal post-diagenetic groundwater alteration and thus reflect the paleo-pH of the La Jolla Profile. Alternatively, there could have been late diagenetic groundwater alteration with acidic fluids, but we find this hypothesis less likely due to the dearth of evidence representing early diagenetic intense weathering conditions. Diagenetic additions of recent/modern organic C can inflate the so-called “preserved” organic C (Broz et al., 2023), but enrichments of TOC in uppermost horizons of paleosols are consistent with preservation of endogenous organic C (Broz et al., 2022). Thus, it is possible that organic C and paleo-pH were preserved in the La Jolla profile, though additions of small amounts of geologically recent/ modern carbon are possible and perhaps likely.

Cardiff Vertisol paleosol had TOC ranging from 0.019 - 0.074 ( $\pm 0.003$ ) wt. % and pH ranging from 7.373 - 8.907 ( $\pm 0.023$ ) (Table S2). Like modern soil profiles, the organic carbon content was enriched in the surface horizons of paleosols (A and Bt) and subsequently depleted in the lower horizons (C horizon). The Cardiff pH results (pH > 8 in some Btss/C-horizons, Table S4) suggest possible late-stage groundwater alteration (e.g., saltwater brines in shore platform) to increase alkalinity in these profiles, as it is unlikely that Vertisols had such alkaline pH during soil formation unless they formed in relatively dry climates (MAP < ~1000 mm) which would allow for the formation pedogenic carbonate (Broz et al., 2021). Since there was no pedogenic carbonate observed in any of the Cardiff profiles, it is likely that the elevated pH is due to late diagenesis (Lukens et al., 2018). The diagenetic history of these paleosols is outlined in the following section.

### **Diagenetic Alteration**

Burial diagenesis is commonly observed in paleosols and particularly affects pre-Quaternary paleosols. The main diagenetic processes can range from minor (burial decomposition of organic matter) to severe (contact metamorphism) (Retallack, 2001). Four

types of diagenetic alteration that have affected paleosols in this work are burial reddening, illitization of smectite, burial gleization, and burial decomposition of organic matter.

The diagenetic process of burial reddening refers to the dehydration of Fe oxyhydroxides (e.g., goethite, ferrihydrite) and subsequent formation of Fe oxides such as hematite (Spinola et al., 2018). This most likely affected the Cardiff Vertisol profiles (**Figure 3**). Modern smectite-rich Vertisols are commonly dark brown to orange in color due to accumulation of goethite and Mn-bearing phases (Driese et al., 2000; Soil Survey Staff, 2014) rather than the brick-red Cardiff paleosol profiles. Alternatively, the Fe oxide minerals may not have formed from burial diagenesis and instead formed during pedogenic alteration before burial, but such accumulation of Fe oxide and subsequent red color is more characteristic of well-drained, highly weathered, non shrink-swell soils (Ultisols, Oxisols) rather than Al/Fe smectite-bearing Vertisols (Chen et al., 2018; Driese et al., 2018).

Illitization of smectite (potash metasomatism) is common in paleosols that are subject to burial diagenesis (Novoselov et al., 2015; Fedo et al., 1995) and involves the incorporation of K into the crystalline structure of smectite clays such as montmorillonite and nontronite (Li et al., 2016; Broz et al., 2022). Evidence for illitization of smectite in the La Jolla kaolinitic profiles included VNIR absorbance features at ~2.35 microns (Figure 8), which is consistent with mixtures of kaolinite and illite (Bishop et al., 2008; Ehlmann et al., 2011) or a mixed layer illite-smectite clay. Alternatively, illite can be derived from the weathering of muscovite and not formed from metasomatic processes (Ehlmann et al., 2011), so caution is necessary in interpreting the origin of illite in these profiles. In any case, further analytical work (e.g., quantitative x-ray diffraction) is needed to support the hypothesis of diagenetic illite in profiles examined in this work.

The striking green-red mottling observed in the paleosurface horizons of the Cardiff paleosols likely resulted from alteration after burial. Burial gleization, a form of early diagenesis, is thought to result from microbial reduction of Fe oxides under hypoxic or anoxic conditions shortly after burial (PiPujol and Buurman, 1994; Retallack, 2019). It most commonly manifests as green-gray color mottling and is restricted to the paleosurface horizons where organic matter is concentrated (e.g., A-horizons). It can be distinguished from groundwater alteration or other primary redoximorphic features by its confinement to the A-horizon of paleosols (PiPujol and Buurman, 1994), whereas groundwater alteration from a fluctuating water table introduces gley colors to the lower parts of the profile (B and C horizons) (Retallack, 1991, 2019).

Burial decomposition of organic matter affects most all paleosols, but is more pronounced in those forming under oxidizing, well-drained conditions before burial (Retallack, 2019; Broz, 2020). This phenomenon, which is thought to be a form of early diagenesis, can lead to severe losses of organic carbon in profiles that were once rich in organic matter. We observed evidence of burial decomposition of carbon because the TOC in all samples (< 0.1 wt.%) was two to three orders of magnitude lower than would be expected



in comparable modern Ultisols and Vertisols of subtropical climates (Broz, 2020). Redox state before burial, inferred from the ratio of FeO/ Fe<sub>2</sub>O<sub>3</sub>, is related to the TOC content of paleosols (Broz, 2020) and can provide a first-order control on the preservation of organic carbon in ancient soils. Generally paleosols forming under reducing conditions (FeO/ Fe<sub>2</sub>O<sub>3</sub> > 0.5) have significantly higher TOC relative to more oxidized profiles with FeO/ Fe<sub>2</sub>O<sub>3</sub> < 0.5 (Broz, 2020). Indeed, samples with higher FeO/Fe<sub>2</sub>O<sub>3</sub> such as the surface (A) horizon of the La Jolla paleosol (*Hwatt*, Figure 11) had significantly more organic carbon (~0.07 wt. TOC %) (**Table S4**) relative to samples with lower FeO/ Fe<sub>2</sub>O<sub>3</sub>, (~0.03 wt. %) providing additional evidence that redox state before burial is related to organic preservation in paleosols.

A summary of the soil forming factors is provided in Table 1. Kaolinite-bearing *Hwatt* and *Mshap* profiles at La Jolla were similar to Aquepts and Tropepts in US Soil taxonomy with bleached surfaced horizons and weakly developed (Bw) subsurface clay horizons characteristic of a seasonally wet coastal lowland landscapes. Similar soils with CIA >95 and bleached surface horizons form under warm, humid and everwet conditions characteristic of single-tier tropical forests. Poorly drained *Hwatt* paleosols could have formed beneath a seasonally dry swamp forest in a wet coastal lowland whereas the *Mshap* profiles on well-drained alluvial terraces supporting a single tier tropical forest. *Psiiw* and *Hamulh* Vertisol paleosols at Cardiff likely formed under warm, humid and seasonally dry conditions on a parent material of quartzofeldspathic silt/ sand and possibly supported a tropical seasonally dry woodland.

Table 1. Summary of La Jolla and Cardiff paleosol interpretations

<b>Pedotype</b>	<b>Location</b>	<b>Soil Taxonomy</b>	<b>FAO Map</b>	<b>Australia</b>	<b>Climate</b>	<b>Organisms</b>	<b>Topography</b>	<b>Parent Material</b>
"Hwatt" "Red"	La Jolla	Aquult	Dystric Gleyisol	Humic Gley	Not diagnostic	Seasonally dry swamp forest	Seasonally wet coastal lowland	Conglomerate
"Mshap" "White"	La Jolla	Aquult	Dystric Cambisol	Brown Earth	Humid, everwet Warm, humid, seasonally dry	Tropical forest, single tier	Well-drained alluvial terrace	Conglomerate
"Psiiw" "Green"	Cardiff	Vertisol	Vertisol	Red Clay	Warm, humid, seasonally dry	Seasonally dry tropical woodland	Well-drained coastal terrace	Quartzofelspathic silt and sand
"Psiiw" "Green"	Cardiff	Vertisol	Vertisol	Red Clay	Warm, humid, seasonally dry	Seasonally dry tropical woodland	Well-drained coastal terrace	Quartzofelspathic silt and sand
"Ha mulh" "Surf"	Cardiff	Vertisol	Vertisol	Red Clay	Warm, humid, seasonally dry	Seasonally dry tropical woodland	Well-drained coastal terrace	Quartzofelspathic silt and sand

### **Geochemical climofunctions and implications for early Eocene climate**

Paleoclimate estimates relating CIA-K (chemical index of alteration minus potassium) to mean annual precipitation (Sheldon et al 2016) are shown in Table 2. We used CIA-K to account for the possible influence of potash metasomatism (illitization of smectite) on CIA values (Novoselov et al., 2015). Samples from the Bt horizon of the Paleocene-Eocene Thermal Maximum (PETM, 55 Ma) profile in La Jolla yielded mean annual temperature (MAT) estimates of  $17.5-17.7^{\circ}\text{C} \pm 4.4^{\circ}\text{C}$  and mean annual precipitation (MAP) of  $1779-1808\text{ mm} \pm 172\text{ mm}$ , consistent with a humid subtropical climate. The early Eocene Climatic Optimum (EECO, 50 Ma) profiles in Cardiff yielded MAT estimates of  $19.8-20.6^{\circ}\text{C} \pm 4.4^{\circ}\text{C}$  and mean annual precipitation (MAP) of  $1186-1280\text{ mm} \pm 172\text{ mm}$ , also consistent with a subtropical humid climate. Evidence for seasonality of precipitation was inferred from vertic features including large sand-filled mudcracks, suggesting a summer-dry EECO climate.

Paleoprecipitation was estimated using the CALMAG transfer function, specifically designed for use in Vertisol paleosols (Nordt and Driese et al., 2010). The Cardiff Vertisols had higher estimated MAP values ranging from  $1494-1565 \pm 108\text{ mm/yr}$ . This is consistent with the phenomenon of underestimation of paleoprecipitation using CIA-K in Vertisols of wet climates (Nordt and Driese, 2010). Together, these estimates suggest a possibly everwet tropical PETM paleoclimate that became warmer and drier in the EECO. Paleoclimate estimates of both localities therefore provide additional evidence of multiple episodes of warm and wet tropical Eocene climates.

**Table 2. Geochemical climofunctions from A and B horizons of early Eocene (55 Ma) paleosol from La Jolla, CA and Eocene (50 Ma) paleosols from Cardiff, CA.** Chemical index of alteration (CIA) and plagioclase index of alteration (PIA) were used to calculate estimates of paleotemperature (error) and paleoprecipitation during soil formation using transfer functions outlined in Sheldon et al (2016) based on a database of modern soils ( $R^2 = 0.72$ ,  $s.e = 182$  mm). The CALMAG weathering index, designed for use with Vertisol paleosols (Norse and Driese, 2010), is defined as  $Al_2O_3/(Al_2O_3 + CaO + MgO) \times 100$  and the resulting transfer function ( $R^2 = 0.9$ ,  $s.e. = 108$  mm) was compared with CIA-K paleoprecipitation estimates (Sheldon et al., 2016).

Location	Age (Ma)	Depth (cm)	Horizon	CIA	CIA-K	CALMAG	Paleotemp. (°C, Sheldon et al. 2002)	Paleoprecip. (mm/yr) Sheldon et al. 2002)	CALMAG paleoprecip. (mm/yr)
La Jolla	55	10	Btg	96.2	96.8	97.6	17.7	1724.8	1779.7
La Jolla	55	18	Btg	98.4	99.3	98.8	17.5	1902.7	1805.9
Cardiff	50	25	Btss	75.4	79.3	83.9	20.9	1186.8	1467.5
Cardiff	50	35	Btss	73.5	77.3	84.1	20.8	1191.9	1473.4
Cardiff	50	60	Btss	83.3	87.0	87.6	19.9	1266.4	1552.2
Cardiff	50	15	Btss	81.1	86.2	88.2	19.8	1280.2	1565.0
Cardiff	50	20	Btss	77.2	81.3	85.1	20.6	1210.0	1494.1
Cardiff	50	35	Btss	79.3	84.2	87.1	20.0	1255.0	1541.2

The range of early Eocene rainfall and temperature estimates presented in this work are consistent with previous calculations of paleotemperature and precipitation from early Eocene fossils and paleosols. These include CIA-K derives estimates of temperature from PETM paleosols in Argentina ( $15\text{ °C} \pm 4.4\text{ °C}$ , Andrews et al., 2017) and fossil leaf-margin derived analysis from Bighorn Basin, Wyoming of  $19.8 \pm 3.1\text{ °C}$ . Additional estimations from fossil flora of the middle Wasatchian (~52 Ma) in Wyoming range from MAT of  $21\text{ °C}$  and MAP of nearly 1400 mm (Wilf, 2000) are closer to the Cardiff Vertisol paleosols (Table 2). From a mineralogical perspective, the presence of potentially abundant kaolinite in La Jolla paleosols (Figure 8) is also similar to PETM paleosols from Texas (White and Schiebout, 2008), Argentina (Sol Raigemborn et al., 2022) and Australia (Zhou et al., 2015).

The seasonally dry and Al smectite- dominated Cardiff Vertisols are consistent with a decrease in MAP (Table 2) after the PETM and seasonality of precipitation at paleolatitudes of 35-45° N during the EECO (Hyland et al., 2018). Estimations of climate from early Eocene coastal paleosols of Southern California therefore provide a new locality for paleoclimate reconstructions as well as for quantifying the nature and intensity of early Eocene weathering on land in present-day southern California.

## **Conclusion**

Deeply weathered paleosols from the Eocene (55 Ma) Mt. Soledad Formation and the Eocene (50 Ma) Delmar formation near San Diego, CA provide new evidence of a subtropical humid climate in southern California during and after the Paleocene-Eocene thermal maximum. Early Eocene (~55 Ma) kaolinitic Ultisol paleosols developed in volcanoclastic conglomerates were subject to intense subaerial alteration and leaching with CIA-K near 99, MAT of  $\sim 17^{\circ}\text{C} \pm 4.4^{\circ}\text{C}$  and MAP of  $\sim 1920 \pm 182$  mm, characteristic of severe weathering under subhumid tropical conditions for thousands of years. Geologically younger Early Eocene (50 Ma) smectitic Vertisol paleosols developed atop coarse sandstones are also intensely weathered (CIA >80) and yield MAT estimates of  $\sim 20^{\circ}\text{C} \pm 4.4^{\circ}\text{C}$  but with lower estimated MAP ( $\sim 1500 \pm 108$  mm) and evidence for seasonality of precipitation. This may have been due to a decline in weathering intensity over ~5 Ma, or a difference in soil-forming factors other than climate such as topography or time of formation. Paleosols examined in this work represent maximum sea level regression in the Eocene of present-day southern California and also reveal a CO<sub>2</sub> greenhouse spike of tropical weathering conditions on land surfaces.

## **Acknowledgements**

Pat Abbot provided invaluable guidance and knowledge in support of this project. Discussions with Briony Horgan, Clemont Royer, Roger Wiens, Jeff Johnson and Candice Bedford aided with data interpretations. Margaret Field assisted with *Kumeyaay* translation. We are also grateful for Emily Huckstead who assisted with laboratory measurements.

## **References**

- Abbott, P.L., 1981, Cenozoic Paleosols of the San Diego Area, California: *Catena*, v. 8, p. 223–237.
- Abbott, P.L., Diego, S., and Smith, T.E., 1989, Sonora, Mexico, source for the Eocene Poway Conglomerate of southern California: *Geology*, v. 17, p. 329–332.
- Abbott, P.L., and Jeffrey A. May, 1991, Eocene Geologic History: San Diego Region: SEPM Pacific Section.
- Anagnostou, E. et al. Changing atmospheric CO<sub>2</sub> concentration was the primary driver of early Cenozoic climate. *Nature* 533, 380–384 (2016).
- Andrews, E., White, T., and del Papa, C., 2017, Paleosol-based paleoclimate reconstruction of the Paleocene-Eocene Thermal Maximum, northern Argentina: *Palaeogeography, Palaeoclimatology, Palaeoecology*, v. 471, p. 181–195, doi:10.1016/j.palaeo.2017.01.042.
- Bishop, J.L., Lane, M.D., Dyar, M.D., and Brown, A.J., 2008, Reflectance and emission spectroscopy study of four groups of phyllosilicates: smectites, kaolinite-serpentines, chlorites and micas: *Clay Minerals*, v. 43, p. 35–54, doi:10.1180/claymin.2008.043.1.03.
- Bowen, G.J., Maibauer, B.J., Kraus, M.J., Röhl, U., Westerhold, T., Steimke, A., Gingerich, P.D., Wing, S.L., and Clyde, W.C., 2014, Two massive, rapid releases of carbon during the onset of the Palaeocene-Eocene thermal maximum: *Nature Geoscience*, v. 8, p. 44–47,

- doi:10.1038/ngeo2316.
- Brimhall, G.H., and Dietrich, W.E., 1987, Constitutive mass balance relations between chemical composition, volume, density, porosity, and strain in metasomatic hydrochemical systems: Results on weathering and pedogenesis: *Geochimica et Cosmochimica Acta*, v. 51, p. 567–587, doi:10.1016/0016-7037(87)90070-6.
- Brown, D.J., Shepherd, K.D., Walsh, M.G., Mays, M.D., and Reinsch, T.G., 2006, Global soil characterization with VNIR diffuse reflectance spectroscopy: *Geoderma*, v. 132, p. 273–290, doi:10.1016/j.geoderma.2005.04.025.
- Broz, A.P., 2020, Organic Matter Preservation in Ancient Soils of Earth and Mars: *Life*, v. 10, doi:doi:10.3390/life10070113.
- Broz, A.P., Clark, J., Sutter, B., Ming, D.W., Tu, V., Horgan, B., and Silva, L.C.R., 2022, Mineralogy and diagenesis of Mars-analog paleosols from eastern Oregon, USA: *Icarus*, v. 380, p. 114965, doi:10.1016/j.icarus.2022.114965.
- Broz, A. P. *et al.* Detection of organic carbon in Mars-analog paleosols with thermal and evolved gas analysis. *J. Geophys. Res. Planets* (2022)  
doi:https://doi.org/10.1029/2022JE007340.
- Broz, A., Aguilar, J., Xu, X. & Silva, L. C. R. Accumulation of radiocarbon in ancient landscapes: A small but significant input of unknown origin. *Sci. Rep.* **13**, 1–12 (2023).
- Chen, C., Barcellos, D., Richter, D.D., Schroeder, P.A., and Thompson, A., 2018, Redoximorphic Bt horizons of the Calhoun CZO soils exhibit depth-dependent iron-oxide crystallinity: *Journal of Soils and Sediments*,.
- Drese, S.G., Simpson, E.L., Eriksson, K.A., and Block, E., 1995, Redoximorphic paleosols in alluvial and lacustrine deposits, 1.8 Ga Lochness Formation, Mount Isa, Australia: Pedogenic Processes and Implications for Paleoclimate: *Journal of Sedimentary Research*, p. 675–679.
- Driese, S.G., and Foreman, J.L., 1992, Paleopedology and paleoclimatic implications of late Ordovician vertic paleosols, Juniata Formation, southern Appalachians: *Journal of Sedimentary Petrology*, v. 62, p. 71–83, doi:10.1306/D4267893-2B26-11D7-8648000102C1865D.
- Driese, S.G., Medaris, L.G., Kirsimäe, K., Somelar, P., and Stinchcomb, G.E., 2018, Oxisolic processes and geochemical constraints on duration of weathering for Neoproterozoic Baltic paleosol: *Precambrian Research*, v. 310, p. 165–178, doi:10.1016/j.precamres.2018.02.020.
- Driese, S.G., Mora, C.I., Stiles, C.A., Joeckel, R.M., and Nordt, L.C., 2000, Mass-balance reconstruction of a modern Vertisol : implications for interpreting the geochemistry and burial alteration of paleo-Vertisols: *Geoderma*, v. 95, p. 179–204.
- Driese, S.G., and Ober, E.G., 2005, Paleopedologic and paleohydrologic records of precipitation seasonality from early Pennsylvanian “Underclay” paleosols, U.S.A: *Journal of Sedimentary Research*, v. 75, p. 997–1010, doi:10.2110/jsr.2005.075.
- Ehlmann, B.L., Mustard, J.F., Clark, R.N., Swayze, G.A., and Murchie, S.L., 2011, Evidence for low-grade metamorphism, hydrothermal alteration, and diagenesis on mars from phyllosilicate mineral assemblages: *Clays and Clay Minerals*, v. 59, p. 359–377, doi:10.1346/CCMN.2011.0590402.
- Field, M., 2012, Kumeyaay language variation, group identity, and the land: *International*

- Journal of American Linguistics, v. 78, p. 557–573, doi:10.1086/667451.
- Fredericksen, N., 1991, Age determinations for Eocene formations of the San Diego California area based on pollen data: SEPM Pacific Section, p. 195.
- Goudge, T.A., Mustard, J.F., Head, J.W., Fassett, C.I., and Sandra, M., 2015, Assessing the Mineralogy of the Watershed and Fan Deposits of the Jezero Crater Paleolake System , Mars: Journal of Geophysical Research – Planets, doi:10.1002/2014JE004782.
- Haber, J.T., Horgan, B., Fraeman, A.A., Johnson, J.R., Wellington, D., Cloutis, E., and Jacob, S., 2022, Mineralogy of a Possible Ancient Lakeshore in the Sutton Island Member of Mt . Sharp , Gale Crater , Mars , From Mastcam Multispectral Images: Journal of Geophysical Research: Planets, v. 127, doi:10.1029/2022JE007357.
- Harris, D., Horváth, W.R., and van Kessel, C., 2001, Acid fumigation of soils to remove carbonates prior to total organic carbon or CARBON-13 isotopic analysis: Soil Science Society of America Journal, v. 65, p. 1853–1856, doi:10.2136/sssaj2001.1853.
- Hyland, E. G., Huntington, K. W., Sheldon, N. D. & Reichgelt, T. Temperature seasonality in the North American continental interior during the Early Eocene Climatic Optimum. *Clim. Past* **14**, 1391–1404 (2018).
- Kennedy, M.P., and Moore, G.W., 1971, Stratigraphic Relations of Upper Cretaceous and Eocene Formations, Son Diego Coastal Area , California. American Association of Petroleum Geologists Bulletin, v. 5, p. 709–722.
- Kovda, I. & Mermut, A. R. *Vertic Features. Interpretation of Micromorphological Features of Soils and Regoliths* (Elsevier B.V., 2018). doi:10.1016/b978-0-444-63522-8.00021-8.
- Kraus, M.J., McInerney, F.A., Wing, S.L., Secord, R., Baczynski, A.A., and Bloch, J.I., 2013, Paleohydrologic response to continental warming during the Paleocene-Eocene Thermal Maximum, Bighorn Basin, Wyoming: Palaeogeography, Palaeoclimatology, Palaeoecology, v. 370, p. 196–208, doi:10.1016/j.palaeo.2012.12.008.
- Kraus, M. J. & Riggins, S. Transient drying during the Paleocene-Eocene Thermal Maximum (PETM): Analysis of paleosols in the bighorn basin, Wyoming. *Palaeogeogr. Palaeoclimatol. Palaeoecol.* **245**, 444–461 (2007).
- Kühn, P., Aguilar, J., Miedema, R. & Bronnikova, M. *Textural Pedofeatures and Related Horizons. Interpretation of Micromorphological Features of Soils and Regoliths* (Elsevier B.V., 2018). doi:10.1016/b978-0-444-63522-8.00014-0.
- Lawrence, C., Harden, J. & Maher, K. Modeling the influence of organic acids on soil weathering. *Geochim. Cosmochim. Acta* **139**, 487–507 (2014).
- Li, Y., Cai, J., Song, M., Ji, J., and Bao, Y., 2016, Influence of organic matter on smectite illitization : A comparison between red and dark mudstones from the Dongying Depression , China: American Mineralogist, v. 101, p. 134–145.
- Ludka, B.C. et al., 2019, Sixteen years of bathymetry and waves at San Diego beaches: Nature Scientific Data, v. 6, p. 1–13, doi:10.1038/s41597-019-0167-6.
- Lukens, W.E., Nordt, L.C., Stinchcomb, G.E., Driese, S.G., and Tubbs, J.D., 2018, Reconstructing pH of paleosols using geochemical proxies: Journal of Geology, v. 126, p. 427–449, doi:10.1086/697693.
- Murphy, C.P., 1983, Point counting pores and illuvial clay in thin section: Geoderma, v. 31, p. 133–150, doi:10.1016/0016-7061(83)90004-6.
- Nesbitt, H. & Young, G. . Early Proterozoic climates and plate motions inferred from major

- elements chemistry of lutites. *Nature* **299**, 715–717 (1982).
- Nordt, L.C., and Driese, S.D., 2010, New weathering index improves paleorainfall estimates from Vertisols: *Geology*, v. 38, p. 407–410, doi:10.1130/G30689.1.
- Novoselov, A.A., Roberto, C., and Filho, D.S., 2015, Potassium metasomatism of Precambrian paleosols: *Precambrian Research*, v. 262, p. 67–83, doi:10.1016/j.precamres.2015.02.024.
- Pearson, P. N. & Palmer, M. R. Atmospheric carbon dioxide concentrations over the past 60 million years. *Nature* **406**, 695–699 (2000).
- Peterson, G., and Abbott, P., 1979, Mid-eocene climatic change, southwestern california and northwestern baja california: *Paleogeography, Paleoclimatology, Paleoecology*, v. 26, p. 73–87.
- PiPujol, M.D., and Buurman, P., 1994, The distinction between ground-water gley and surface-water gley phenomena in Tertiary paleosols of the Ebro basin, NE Spain: *Palaeogeography, Palaeoclimatology, Palaeoecology*, v. 110, p. 103–113, doi:10.1016/0031-0182(94)90112-0.
- Retallack, G.J., 2009, Cambrian paleosols and landscapes of South Australia: *Australian Journal of Earth Sciences*, p. 37–41, doi:10.1080/08120090802266568.
- Retallack, G.J., 2019, *Soil of the Past*: Wiley Blackwell.
- Retallack, G.J., 1991, Untangling the effects of burial alteration and ancient soil formation: *Annual Review of Earth and Planetary Sciences*, p. 183–206.
- Retallack, G.J., Bestland, E., and Fremd, T., 2000, Eocene and Oligocene Paleosols of Central Oregon: *Geological Society of America Special Paper*, v. 344, p. 1–192, doi:10.1046/j.1365-3091.2001.0394c.x.
- Sheldon, N.D., Retallack, G.J., and Tanaka, S., 2002, Geochemical Climofunctions from North American Soils and Application to Paleosols across the Eocene - Oligocene Boundary in Oregon: *The Journal of Geology*, v. 110, p. 687–696, doi:10.1086/342865.
- Smith, M.E., Carroll, A.R., and Singer, B.S., 2008, Synoptic reconstruction of a major ancient lake system : Eocene Green River Formation , western United States: *GSA Bulletin*, p. 54–84, doi:10.1130/B26073.1.
- Sol Raigemborn, M., Lizzoli, S., Hyland, E., Cotton, J., Gómez Peral, L.E., Beilinson, E., and Krause, J.M., 2022, A paleopedological approach to understanding Eocene environmental conditions in southern Patagonia, Argentina: *Palaeogeography, Palaeoclimatology, Palaeoecology*, v. 601, doi:10.1016/j.palaeo.2022.111129.
- Song, B., Zhang, K., Zhang, L., Ji, J., Hong, H., Wei, Y., Xu, Y., Algeo, T.J., and Wang, C., 2018, Qaidam Basin paleosols reflect climate and weathering intensity on the northeastern Tibetan Plateau during the Early Eocene Climatic Optimum: *Palaeogeography, Palaeoclimatology, Palaeoecology*, v. 512, p. 6–22, doi:10.1016/j.palaeo.2018.03.027.
- Spinola, D.N., Portes, R. de C., Srivastava, P., Torrent, J., Barrón, V., and Kühn, P., 2018, Diagenetic reddening of Early Eocene paleosols on King George Island, Antarctica: *Geoderma*, v. 315, p. 149–159, doi:10.1016/j.geoderma.2017.11.010.
- Staff, S.S., 2014, *Keys to Soil Taxonomy*: United States Department of Agriculture, v. 12.
- White, P.D., and Schiebout, J., 2008, Paleogene paleosols and changes in pedogenesis during the initial Eocene thermal maximum : Big Bend National Park , Texas , USA C24r: GSA

*This paper is a non-peer reviewed preprint submitted to EarthArXiv.*

Bulletin, p. 1347–1361, doi:10.1130/B25987.1.

Wilf, P., 2000, Late paleocene-early eocene climate changes in Southwestern Wyoming: Paleobotanical analysis: Bulletin of the Geological Society of America, v. 112, p. 292–307, doi:10.1130/0016-7606(2000)112<292:LPECCI>2.0.CO;2.

Zachos, J.C., Dickens, G.R., and Zeebe, R.E., 2008, An early Cenozoic perspective on greenhouse warming and carbon-cycle dynamics: Nature, v. 451, p. 279–283, doi:10.1038/nature06588.

Zhou, Y., Retallack, G.J., and Huang, C., 2015, Early Eocene paleosol developed from basalt in southeastern Australia: implications for paleoclimate: Arabian Journal of Geosciences, v. 8, p. 1281–1290, doi:10.1007/s12517-014-1328-8.